JOURNAL OF GEOPHYSICAL RESEARCH, VOL. 102, NO. A5, PAGES 9705-9716, MAY 1, 1997

Ions and electrons of the lower-latitude *D* region

A. Kull[1] and E. Kopp
Physikalisches Institut der Universität Bern, Bern, Switzerland

C. Granier and G. Brasseur
National Center of Atmospheric Research, Boulder, Colorado

Abstract. A positive and negative ion chemical steady state model which combines about 400 ion-chemical and photochemical reactions with a two-dimensional neutral model for minor atmospheric constituents is presented in the height range 50–84 km, for latitudes −50° to +50° in January and September. The ion model yields concentrations of the main positive and negative ions and of electrons. Two important parameters for the description of the lower ionosphere were deduced, namely, the ratio λ of electrons to negative ions and the f^+ parameter, describing the ratio of the positive cluster ions to positive molecular ions. In addition, the parameterization of f^+ indicates a strong dependency on the water vapor concentration. At the transition height ($f^+ = 1$) at midlatitudes the water concentration can be expressed as a function of the electron density and the temperature: $[H_2O] = 1.09 \times 10^{-6}[\rho]^{0.6}T^{-3}[e]$, with the units of the water vapor density $[H_2O]$, the air density $[\rho]$, and the electron concentration $[e]$ in cm^{-3} and T in degree kelvin.

1. Introduction

The knowledge of positive and negative ion composition in the lower ionosphere of the *D* region is only based on a limited number of rocket flights for the past 30 years with measurements from cryogenically pumped mass spectrometers. After the first *D* region positive ion composition measurements by *Narcisi and Bailey* [1965] it became evident that instead of NO^+ and O_2^+, the hydrated ions of oxonium, commonly named proton hydrates, are the dominant positive ions in the *D* region. After this striking observation, *Fehsenfeld and Ferguson* [1969] and *Ferguson and Fehsenfeld* [1969] have started to explain the formation of proton hydrates with two sets of reactions, the so-called hydration chains of NO^+ and O_2^+. These reactions become active particularly below a certain altitude in the mesosphere, which is known as the transition height. At the transition height the concentration of the two molecular ions NO^+ and O_2^+ is equal to the sum of the proton hydrates and below this height the proton hydrates become dominant. The exact reaction chains for the formation of proton hydrates were studied in various laboratories beginning in the early 1970s until the late 1980s. Particularly important were those kinetic measurements made at temperatures relevant to the mesosphere between 100 and 200 K, which was important for modeling of the transition height and the formation of proton hydrates with higher hydration orders (n = 4–7). Besides the temperature, the three minor constituents NO, $O(^3P)$, and H_2O determine the ratio of NO^+/O_2^+, the formation of $H^+(H_2O)_2$ from the O_2^+ hydration, and $H^+(H_2O)_3$ from the NO^+ hydration, respectively.

Using the set of available laboratory reaction rate constants, many ion chemical steady state model analyses of the positive ion composition in the *D* region have been made to explain the variability of the transition height and the role of temperature, nitric oxide, and water vapor concentrations for the distribution of positive ions in the *D* region [*Reid*, 1977; *Thomas*, 1983; *Koshelev*, 1987]. *Kopp and Herrmann* [1984] proposed a parameterization of the density ratio f^+

$$f^+ = \frac{[\text{Clust}^+]}{[NO^+] + [O_2^+]} \tag{1}$$

as a function of the neutral density, the atomic oxygen concentration, temperature, and the electron density.

Brasseur and De Baets [1986] have combined for the first time a steady state ion model (BDB model) with a two-dimensional neutral model to study the seasonal and latitudinal variability of the ion composition and its dependence on the variability of NO, O, H_2O, temperature, and varying ionization sources. The BDB model confirmed nicely the tendencies of positive ion composition variabilities as observed from in situ rocket measurements. However, the model was based on reaction rates, which do not fully contain yet the strong temperature dependence of the three-body type clustering reaction for NO^+, O_2^+, and $NO^+ \cdot X$.

The initial formation of negative ions in the *D* region, as proposed in the BDB and other models by *Wisemberg and Kockarts* [1980] and *Thomas and Bowman* [1985], is first from three-body attachment of electrons to molecular oxygen and second by dissociative electron reaction with ozone forming O_2^- and O^- ions, respectively. Other minor constituents, mainly O_3, OH, HCl, and NO are relevant to the formation of various secondary ions [e.g., *Wisemberg and Kockarts*, 1980]. One important parameter in negative ion models of the *D* region is the parameter λ, the ratio of the sum of negative ions to the concentration of electrons. The atomic oxygen concentration, which has a large variability, and the effect of photodetachment during daytime are the most important parameters. Additionally, the temperature and neutral density affect the parameter λ.

[1]Now at Max-Planck-Institut für Extraterrestrische Physik, Garching, Germany.

Paper number 97JA00327.
0148-0227/97/97JA-00327$09.00

The aim of this calculation is to model the composition of positive and negative ions and the electron density of the D region from 50 to 84 km altitude, and between 50°S and 50°N latitude, using a two-dimensional neutral model [*Granier and Brasseur*, 1992] together with an updated set of relevant ion-chemical reaction rate constants [*Kopp*, 1996]. The lifetime of D region ions against dissociative electron recombination is 60–300 s, which allows us to neglect the process of ion-drag and ion transport by electric fields and neutral winds. The ionization has been restricted to direct photoionization of NO by Lyman α above 60 km with the addition of galactic cosmic ray ionization from 50 to 80 km.

2. Ion Production and Ion Chemistry

The electron-ion pair production in our model calculation of the midlatitude D-region originates from Lyman α (121.6 nm) ionization of nitric oxide above 60 km combined with galactic cosmic rays between 50 and 80 km. The contributions of the direct ionization of $O_2(^1\Delta)$ with UV range 102.7–111.8 nm and Lyman β are neglected. The influence of the 11-year solar cycle variation on the variability of the UV radiation is parameterized through a linear parameter A_{sol} with values between +1 (high solar activity), 0 (medium solar activity) and −1 (low solar activity). The corresponding Lyman α flux ranges from 2×10^{11} cm^{-2} s^{-1} for minimum to 4×10^{11} cm^{-2} s^{-1} for maximum solar activity. The dependence of the nitric oxide ionization rate $P(NO^+)$ on the solar zenith angle χ and on the O_2 column density for different levels of solar activity is taken from *Brasseur and Solomon* [1986].

$$P(NO^+) = (6 + 2 \cdot A_{sol}) \times 10^{-7} \cdot \exp\left[-10^{-20} N(O_2, z, \chi)\right] \text{ s}^{-1} \quad (2)$$

The expression uses the cross sections for the ionization $\sigma(NO) = 2.0 \times 10^{-18}$ cm^{-2} and for the absorption $\sigma(O_2) = 1.0 \times 10^{-20}$ cm^{-2}, respectively. $N(O_{2,z,\chi})$ is the column density above the altitude z along the direction of the solar radiation.

The total ion production Q_{CR} by galactic cosmic rays is distributed between the four different primary ions according to *Rusch et al.* [1981] as $P(N_2^+) = 0.585 Q_{CR}$, $P(N^+) = 0.185 Q_{CR}$, $P(O_2^+) = 0.154 Q_{CR}$ and $P(O^+) = 0.076 Q_{CR}$. For latitudes below 53°, *Heaps* [1978] has determined the following parameterization for the ion production at different latitudes, ϕ and for different levels of solar activity A_{sol}.

$$Q_{CR} = \left[X_1 + \left(X_2 - \frac{A_{sol} - 1}{2}(X_3 - X_2)\right)(\sin\phi)^4\right] \times 10^{-17^{(1-X_4)}} M^{X_4} \text{ cm}^{-3} \text{ s}^{-1} \quad (3)$$

The parameters in this equation are $X_1 = 1.74 \times 10^{-18}$, $X_2 = 1.93 \times 10^{-17}$, $X_3 = 2.84 \times 10^{-17}$, and $X_4 = 0.6 + 0.8\ |\cos\phi|$. For total densities below 3×10^{17} cm^{-3} the parameter X_4 is unity. We assume a linear and negative dependency of the galactic cosmic ray variation with the solar activity over the solar cycle.

A small variation of the ratio NO^+/O_2^+ along its vertical profile is attributed to the loss of molecular oxygen ions from the reaction $O_2^+ + NO \rightarrow NO^+ + O_2$ with nitric oxide. The primary ions, NO^+, O_2^+, N_2^+, O^+, and N^+, are the starting ions for a large variety of different reactions as listed by *Kopp* [1996]. The chemistry for the positive ions is based on the pioneering work of *Reid* [1976, 1977] and *Thomas* [1976a, b] with the detail reaction chain for NO^+ hydration. In contrast to most of the previous models, our proton hydrate formation starts with $H^+(H_2O)_2$ and not with the oxonium ion H_3O^+. *Rakshit and Warneck* [1980] have demonstrated the absence of the H_3O^+-production from the reaction $O_2^+ \cdot (H_2O) + H_2O$ at mesospheric temperatures (100–220 K). *Kopp* [1984] discussed the production of H_3O^+ from the charge exchange reactions of O_2^+ with H_2O_2. Since the hydrogen peroxide molecule and other specific minor constituents as HCN, which contribute to the oxonium ion formation, are not included in the two-dimensional neutral model, the oxonium ion H_3O^+ is ignored in the model.

The complex positive ion chemistry of the D region can be divided in three main sequences, namely, (1) rapid transfer of primary ions NO^+, O_2^+, N_2^+, O^+, and N^+ into the starting ions NO^+ and O_2^+ for the hydration, (2) the two hydration chains $NO^+ \rightarrow NO^+(H_2O)_3 \rightarrow H^+(H_2O)_3$ and $O_2^+ \rightarrow H_3O^+OH \rightarrow H^+(H_2O)_2$, and (3) the formation of higher order proton hydrates $H^+(H_2O)_2 \rightarrow H^+(H_2O)_7$. The positive ion chemistry has been extended by 20 reactions form the model by *Brasseur and De Baets* [1986].

The temperature can enter as a controlling parameter particularly for the clustering reactions of NO^+ and $NO^+ \cdot X$ ($X = H_2O$ and $2H_2O$), for example,

$$NO^+ + N_2 + M \rightarrow NO^+ \cdot N_2 + M \quad (4)$$

$$NO^+ + CO_2 + M \rightarrow NO^+ \cdot CO_2 + M. \quad (5)$$

Equally important, the temperature controls the probability of a collisional induced breakup of cluster ions in the reaction of the type:

$$NO^+ \cdot X + M \rightarrow NO^+ + X + M \quad (X = N_2, CO_2). \quad (6)$$

The efficiency of the O_2^+ hydration is reduced in conditions of high atomic oxygen concentration through

$$O_4^+ + O \rightarrow O_2^+ + O_3. \quad (7)$$

The start of the negative ion formation is a three-body type attachment of electrons to molecular oxygen atoms, and the reaction of electrons with ozone,

$$e + O_3 \rightarrow O^- + O_2. \quad (8)$$

The negative ion part of the ion chemistry involves 36 ion chemical and 11 photochemical reactions. The model is based on the work by *Wisemberg and Kockarts* [1980], *Thomas* [1983], and *Thomas and Bowman* [1985].

3. Neutral Density, Temperature, and Minor Constituents

The neutral model which is used in the present study is described in detail by *Brasseur et al.* [1990] and *Granier and Brasseur* [1992]. The model, which is two-dimensional (latitude, altitude), extends from the surface to the mesopause, with a spatial resolution of 5° in latitude and 1 km in altitude. Chemical, dynamical, and radiative processes are treated interactively above 15 km altitude. Below this level, the distributions of the chemical species are calculated with prescribed temperature, winds, and relative humidity.

Above 15 km altitude, dynamical equations are expressed using the transformed-Eulerian mean formulation, as described by *Andrews and McIntyre* [1976]. Momentum deposi-

tion and eddy diffusivity associated with gravity wave breaking and planetary wave absorption are parameterized as a function of the zonal mean wind and temperature fields. The solar forcing is calculated through an explicit spectral integration of the energy deposited. The net adiabatic heating rate is obtained from the radiative transfer code described by *Briegleb* [1992] below 65 km altitude. Above this level, a Newtonian cooling formulation is adopted.

The chemical scheme includes approximately 60 species belonging to the oxygen, hydrogen, nitrogen, chlorine, and bromine families. It involves about 120 chemical and photochemical reactions. The reactions rates, as well as, the absorption cross-sections used for the calculation of photodissociation rates are taken from *DeMore et al.* [1992]. Values of the solar irradiance are from *Brasseur and Simon* [1981].

The model provides the concentration of trace constituents in addition to the temperature, air density, and wind components. Included are all species which determine the formation and fate of ions in the middle atmosphere.

The nitric oxide density in January is shown in Figure 1. It is a key parameter to determine the ionization rate. The atomic oxygen distribution, which is important for the loss of negative ions, is shown in Figure 2 for a January midday and in Figure 3 for similar daytime condition at equinox. The seasonal dependency of water vapor, which is only pronounced above 70 km, is shown in Figure 4. The midday temperature distribution in January which is used to determine the positive and negative ion compositions is presented in Figure 5.

4. Ion Chemistry Model

The main neutral constituents used for the calculation of the ion distribution are N_2, O_2, CO_2, CH_4, H_2, H_2O, and the photochemically active species, $O(^3P)$, NO, O_3, and H. Presently the ion model is limited to latitudes between 50°S and 50°N and to the altitude range from 50 to 84 km. As already mentioned, ions are produced by the photoionization of direct and scattered Lyman α radiation and the galactic cosmic rays. Primary positive ions from cosmic rays are O^+, O_2^+, N^+, and N_2^+. the ion NO^+ is the product of a direct Lyman α photoionization of NO and is by far the largest fraction of the ionization above 75 km. A set of fast two-body type reactions converts O^+, N^+ and N_2^+ into NO^+ and O_2^+. The primary negative ions O^- and O_2^- originate from dissociative electron attachment to O_3, and three-body attachment to O_2. All possible intermediate clusters of the form $O_2^+ \cdot X$, $NO^+ \cdot X$ and positive hydrates $H^+(H_2O)_{2-7}$ are considered as positive secondary ions. The negative secondary ions are O_3^-, CO_3^-, NO_2^-, OH^-, NO_3^-, CO_4^-, O_4^-, and HCO_3^-.

The ion chemical model in the present study incorporates a total of about 400 ion and photochemical reactions and represents the known *D* region ion chemistry [*Kopp*, 1996]. However, because of the missing density data of $O_2(^1\Delta)$, its ionization by Lyman β is not included. According to *Hunten and McElroy* [1968], this leads to an underestimated total ionization rate of about 5% to 20% between 80 and 84 km. Yet, this underestimation is masked by the uncertainty on the NO density because it enters directly into the total ionization rate as main ionization process by the ionization of NO by Lyman α. We therefore conclude that in the present state of the model calculation, the missing ionization due to the absence of ionization of $O_2(^1\Delta)$ by Lyman β can be neglected because of the uncertainty of the NO density.

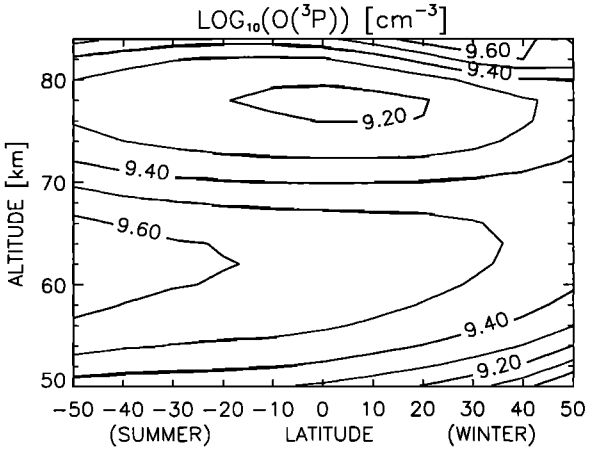

Figure 2. Atomic oxygen density in the *D* region for the height range of 50–84 km and between the latitudes −50° (summer hemisphere) and 50° (winter hemisphere) for January and noon conditions.

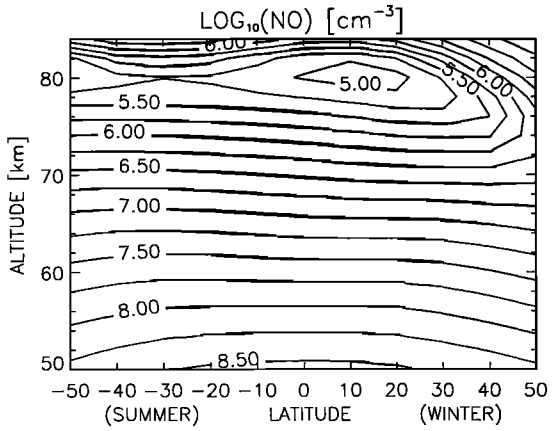

Figure 1. Nitric oxide density in the *D* region for the height range of 50–84 km and between the latitudes −50° (summer hemisphere) and 50° (winter hemisphere) for January and noon conditions.

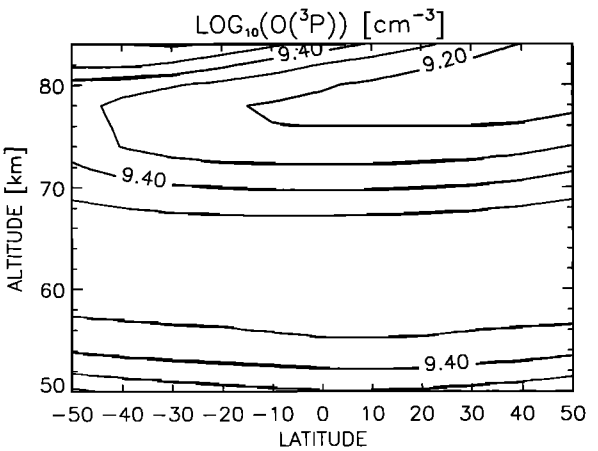

Figure 3. Atomic oxygen density in the *D* region for the height range of 50–84 km and between the latitudes −50° and 50° for equinox (September) and noon conditions.

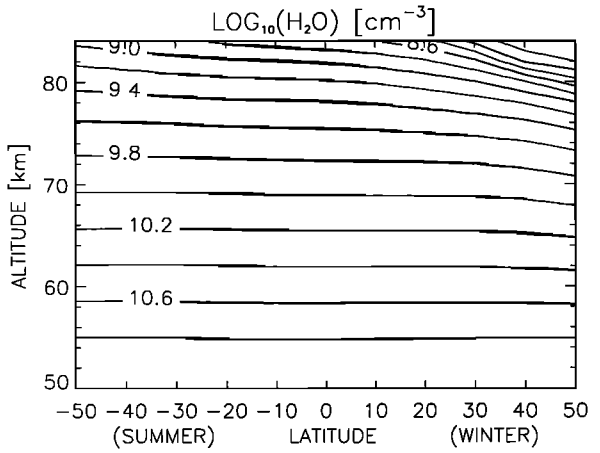

Figure 4. Water vapor density in the *D* region for the height range of 50–84 km and between the latitudes −50° (summer hemisphere) and 50° (winter hemisphere) for January and noon conditions.

The ion composition and ion chemical reaction path of the *D* region are directly coupled to the local concentration of other neutral long-lived trace species such as H_2O, O, and CO_2. Other gases, such as O_3, NO_2, and H are important for the negative ion chemistry. The uncertainties of the main neutral trace constituents have the largest effect on the accuracy of the model results. Few measurements of main trace constituents make it difficult to estimate the uncertainties on related model results. Although the complex qualitative dependencies may be understood in most cases, quantitative analysis is only possible in a few cases. An example for such a case is the pronounced dependency of the f^+ parameter with regard to the water vapor density (see section 7).

The uncertainties in the reaction rate constants also affects model calculations directly. According to laboratory measurements, their uncertainty is within 10% for the positive ion chemistry [*Kopp*, 1996]. The negative ion chemistry reaction rates are much less supported by measurements. Ion families, such as chlorine and its cluster ions, which are not considered in our model, may also play an important role. Uncertainty from the recombination, photodissociation, and photodetachment rates provide the largest errors in the calculation. Recombination leads to the destruction of ions either by positive-negative ion recombination or dissociative recombination of positive ions and electrons. The corresponding rates are based on *Kopp* [1996] and *Millar et al.* [1991]. In general, the recombination rates depend on the *D* region temperature. For recombination rates which were measured without temperature dependency, we used the theoretically expected temperature dependence of the form $T^{-0.5}$. Model calculation showed that the theoretically expected temperature dependency results in higher recombination rates, approximately a factor 1.1–1.3 in regions of the *D* region where the temperatures are low, e.g., below 200 K.

Photodetachment of electrons and photodissociation of molecular ions play an important role for the negative ion chemistry and for the electron density in particular. The corresponding uncertainty in the photodetachment and dissociation rates should be directly associated with the calculated electron density in parts of the *D* region where the negative ion density is high compared to the electron density.

5. Model Calculation

The ion chemistry model that has been used for the present study is characterized by a system of ordinary nonlinear first order differential equations. Unique solutions depending on initial conditions do exist since the problem can be shown to be mathematically well posed. In order to handle the very different timescales, we have applied the stiff integration scheme developed by *Gear* [1971]. Each individual ion chemical reaction corresponds to at least one differential equation. Loss and production rate are computed separately. In this way the charge neutrality equation $N_e + N_- = N_+$ (where N_e denotes the electron, N_- the negative ion, and N_+ the positive ion density) is included automatically and may be used to control the numerical accuracy of the model calculation.

The model at the present stage assumes steady state condition. Most time scales of dynamical processes in the mesosphere are substantially longer than as compared to the chemical processes. The dynamical time scale is of the order of days [*Brasseur and Solomon*, 1986], and the lifetime of ions in the *D* region is only of the order of 100 s or less. As a consequence, the effect of ion transport can be neglected and the assumption of a steady state is fulfilled. The validity of this approach seems to be confirmed by electron density measurements [*Swider and Narcisi*, 1983], by measurements of the total ion density [*Conley*, 1983] and mass spectrometer observations [*Narcisi et al.*, 1983].

6. Results

Presented results originate from steady state calculations of the ion chemical model described above. They refer to latitudes between −50° and 50°, to the height range 50 km to 84 km, and to medium solar activity.

6.1. Ionization Rate

The total *D* region ionization rate for January and noon conditions are presented in Figure 6. Pronounced variations with both height and latitude (winter and summer hemisphere) are observed, leading to a non symmetrical latitude distribution, especially at heights above 70 km. The maximum ionization rate is located at 50° latitude and 84 km. This situation is

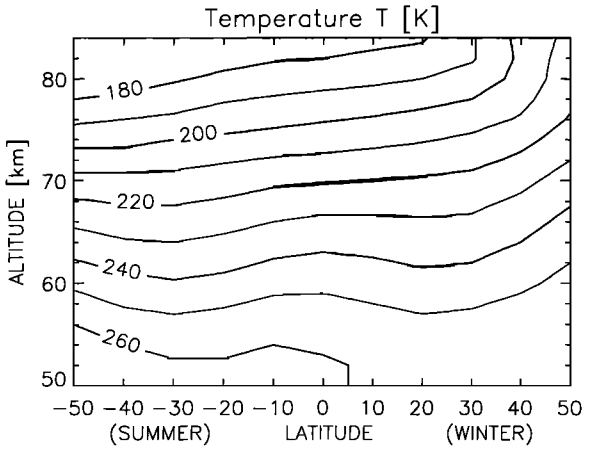

Figure 5. Temperature of the *D* region for the height range of 50–84 km and between the latitudes −50° (summer hemisphere) and 50° (winter hemisphere) for January and noon conditions.

typical for winter conditions since the NO density is relatively high as may be seen in Figure 1. The higher ionization rate above 80 km compared to the region between 70 and 80 km is also related to a higher NO concentration. Between 50 and 65 km, the ionization due to galactic cosmic rays shows a symmetric pattern. Its contribution to the total ionization rate dominates in this region and reveals a pronounced and expected variability with latitude and height, originating from the interaction with the earth magnetic field and the atmospheric density. At heights of about 70 km, both, ionization by galactic cosmic rays and ionization of NO by Lyman α contribute to the total ionization rate. Two local minima of the total ionization rate are found in the summer hemisphere: The first is located at $-30°$ and at about 80 km and is expected to be due to the NO density minimum. The second minima is found at 68 km and marks the boundary between the region dominated by galactic cosmic rays and the region dominated by Lyman α. Only one ionization rate minimum is found in the winter hemisphere. It corresponds to the transition height of the two ionization processes and a minimum of the NO density at the same height. Interpreting Figure 6, one should bear in mind that we have not considered the ionization of $O_2(^1\Delta)$ by Lyman β. This fact leads to a total ionization rate which may be too low above 80 km, particularly in the summer hemisphere.

6.2. Electron Density

The electron density as calculated from the model is shown in Figure 7. In general, its distribution contours resemble those of the total ionization rate. Responding to local minima and maxima of the total ionization rate, the electron density reaches a maximum at a latitude of 50°N at the top of the model range. Localized minima and the corresponding maximum between them are also found in the summer hemisphere but in a less pronounced manner. Similar structures are found below 75 km where the electron density increases with latitude. This reflects a direct dependency of the electron density on the galactic cosmic rays in this region. Above 70 km, ionization of NO by Lyman α starts to dominate the electron density. The most obvious difference between the total ionization rate and the electron density is its steady increase with height. This feature is due to the decrease of mesospheric density, which leads to a lower probability for loss of electrons by three body

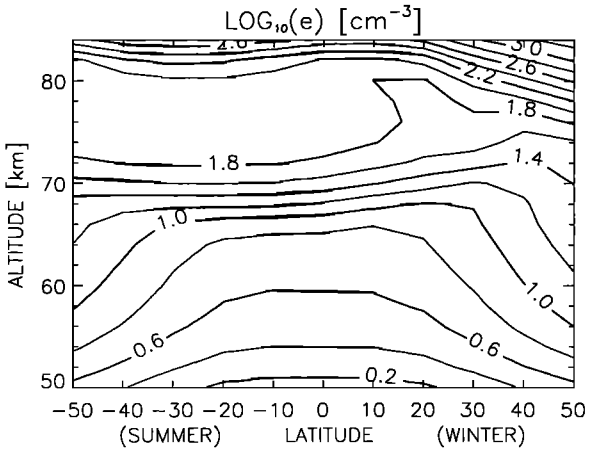

Figure 7. Electron density in the D region for the height range of 50–84 km and between the latitudes $-50°$ (summer hemisphere) and 50° (winter hemisphere) for January and noon conditions.

reactions, involving electrons, O_2 and N_2, and formation the primary negative ion O_2^-. Another effect is obvious from comparison of the electron density and the density of atomic oxygen O (cf. Figure 2). Electron detachment from O_2^- is caused either by photodetachment or by reactions with atomic oxygen. A higher density of atomic oxygen thus corresponds to a higher electron detachment rate. The oxygen minimum that occurs in the same region as the maximum of the total ionization prevents the rapid formation of negative ions, leading to a moderate electron density maximum. Other mesospheric effects are present but are more difficult to identify directly. For example, a higher total recombination rate is observed in regions where proton hydrates dominate the molecular ions. Also, the mesospheric temperature exerts control on electron density through the temperature dependency in the recombination rates.

In Figure 8, the electron concentration for equinox (September) at midday is plotted. As may be expected, the electron density is more symmetric than for January conditions. However, mesospheric effects like higher O and NO concentrations in the southern hemisphere (see Figure 3) lead to higher electron densities in the corresponding region.

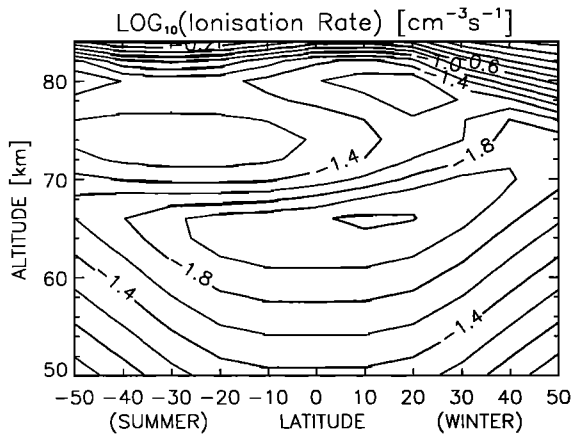

Figure 6. The total D region ionization rate for the height range of 50–84 km and between the latitudes $-50°$ (summer hemisphere) and 50° (winter hemisphere) for January and noon conditions.

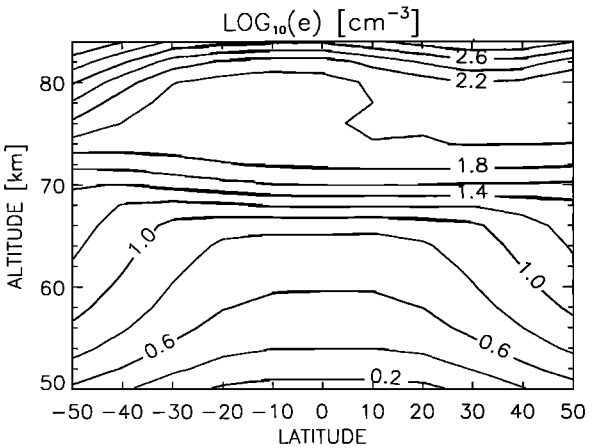

Figure 8. Electron density in the D region for the height range of 50–84 km and between the latitudes $-50°$ and 50° for equinox (September) and noon conditions.

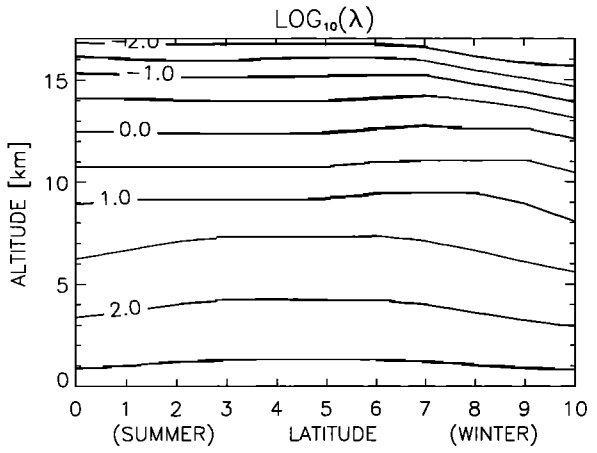

Figure 9. Value of the parameter λ in the *D* region for the height range of 50–84 km and between the latitudes −50° (summer hemisphere) and 50° (winter hemisphere) for January and noon conditions.

6.3. Parameter λ

An important parameter for the negative ion chemistry is the ratio between the total negative ion density and the electron density

$$\lambda = [N_-]/[N_e]. \quad (9)$$

In Figure 9, the λ contour plot is shown for the conditions discussed above. A far less pronounced seasonal dependence than that of the total ionization rate and the electron density is observed. The height dependence is understood as an effect of the decreasing mesospheric density which leads to a lower probability for three-body reactions, and thus to a lower negative ion production rate. The less pronounced latitude dependence indicates similar underlying processes for the electron density and the negative ion concentration. Low variability of λ is seen in the winter hemisphere at heights of about 75 km. Higher mesospheric temperatures in winter (see Figure 5) lead to higher production rates of the primary negative ion, O_2^-, in this season. The altitude of transition between the region dominated by negative ions and the region dominated by electrons is located at about 75 km. Below this level, the electron concentration relative to the negative ion density decreases rapidly to a value 2 orders of magnitude smaller by 55 km altitude.

6.4. Parameter f^+

In Figures 10 and 11, we present contour plots of the parameter f^+, which represents the ratio of the concentration between the positive cluster ions and the total concentration of the molecular ions, O_2^+ and NO^+. The parameter f^+ represents the most useful model parameter for the positive ion chemistry of the *D* region. It marks the transition between the region dominated by molecular ions and the region dominated by proton hydrates. It also denotes a distinct change in the effective electron dissociative recombination rate. Figure 10 corresponds to January and Figure 11 to equinox conditions. Figures 10 and 11 show a decrease of the f^+ values over several orders of magnitude with increasing height. This feature is well understood since the production of cluster ions is based on three-body reactions whose probabilities decrease with the decreasing mesospheric density. Other mesospheric effects also contribute to this tendency. Since an increasing atomic oxygen density leads to a lower density of O_4^+ via the reaction $O_4^+ + O \rightarrow O_2^+ + O_3$ and since O_4^+ represents the starting point of the clustering reaction chain, the increasing atomic oxygen density leads to the decrease of the f^+ parameter. The same may be observed for the increasing electron density which leads to a higher recombination rate and thus to a lower f^+ value. Furthermore, higher mesospheric temperatures in the winter hemisphere above 75 km reduce the cluster production rate and thus lower the f^+ value. Therefore *Kopp and Herrmann* [1984] proposed a parameterization of f^+ as a function of the neutral density, the atomic oxygen density, temperature, and the electron density. These dependencies of f^+ on the electron concentration, the mesospheric temperature and density and the O concentration explain the structures of Figure 10 below 78 km.

Above 78 km, the present model calculations show an additional pronounced dependency of the parameter f^+ on the H_2O density for January conditions. This is particularly recognized in the midlatitude winter hemisphere above 80 km, where the H_2O density tends to decrease toward zero (Figure

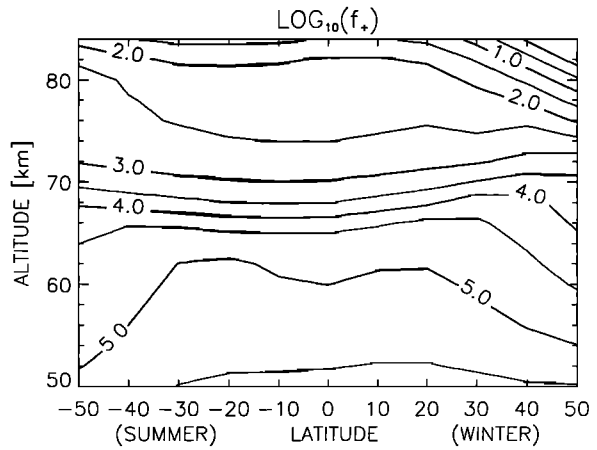

Figure 10. Value of the parameter f^+ in the *D* region for the height range of 50–84 km and between the latitudes −50° (summer hemisphere) and 50° (winter hemisphere) for January and noon conditions.

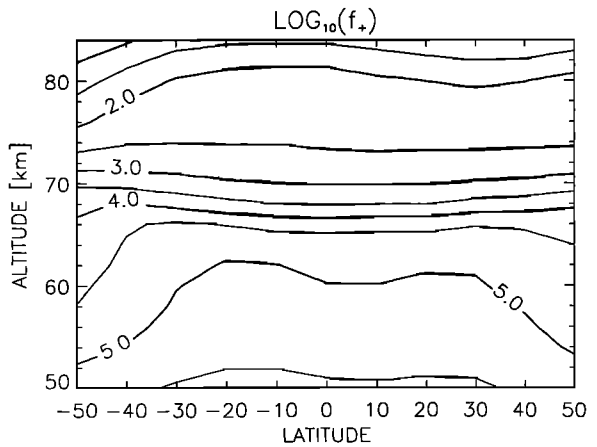

Figure 11. Value of the parameter f^+ in the *D* region for the height range of 50–84 km and between the latitudes −50° and 50° for equinox (September) and noon conditions.

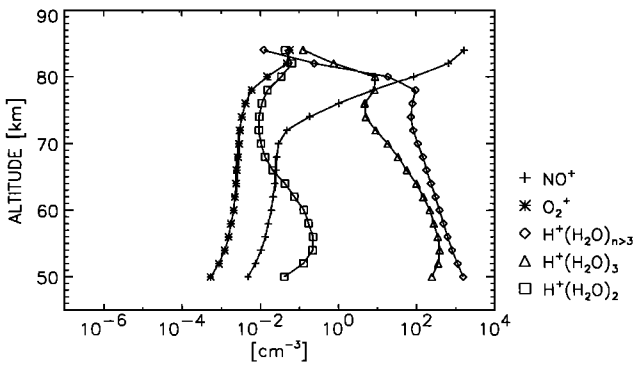

Figure 12. Vertical distribution of selected positive ions at the latitude 50° (winter hemisphere) for the height range of 50–84 km in January and noon conditions.

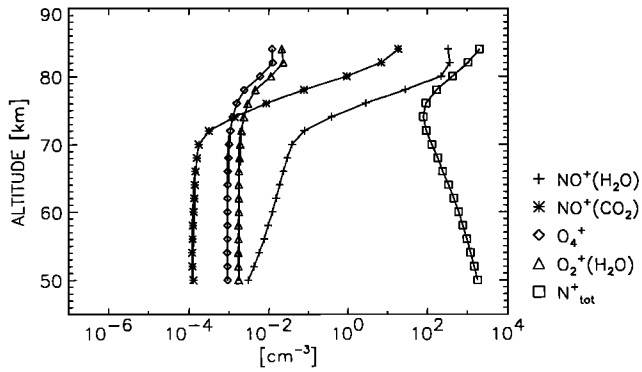

Figure 14. Vertical distribution of selected positive ions at the latitude 50° (winter hemisphere) for the height range of 50–84 km in January and noon conditions.

4). Since H_2O represents one of the main constituents for the clustering chain, an additional dependency of f^+ on the H_2O density becomes important. In section 7, we present an extended study of this dependency in an analytical form.

The contour line for $f^+ = 1$ corresponds to the transition between *D* region and *E* region. In Figure 10, this transition height increases from about 81 km at 50°N to 84 km at the 40°N latitudes and remains above 84 km between 40°N and 50°S.

Below 74 km, the f^+ contour plots for January and September do not differ significantly. However, pronounced differences do occur above 74 km. As expected, the equinox situation presented in Figure 11 is more symmetric than the January situation (Figure 10). In particular, f^+ remains above the value of 1 indicating the dominance of cluster ions. Thus, in the equinox situation, the *D* region extends above 84 km for the whole latitude range under consideration.

6.5. Concentration of Selected Positive Ions

Figure 12–15 show altitude profiles of the positive molecular ions NO^+ and O_2^+, the total positive ions and selected ions of the three main cluster families of the *D* region, $NO^+ \cdot X$, $O_2^+ \cdot X$, and the proton hydrates $H^+(H_2O)_n$. The profiles correspond to midday January conditions in winter (+50°) and summer (−50°). Height profiles of the most important cluster ions $NO^+(H_2O)$ and $NO^+(CO_2)$ in the $NO^+ \cdot X$ family and $O_2^+(H_2O)$ and O_4^+ in the $O_2^+ \cdot X$ family, are shown in Figures 14 and 15. The less abundant cluster ions (<1 cm^{-3}) NO^+N_2 and $NO^+(H_2O)_2$ and $NO^+(H_2O)_3$, for which the mass spectrometer has not enough sensitivity, are not shown. In the proton hydrate family height profiles of $H^+(H_2O)_2$, the final ion from O_2^+ hydration, $H^+(H_2O)_3$ from the NO^+ hydration, and $H^+(H_2O)_{n>3}$ resulting from further clustering of $H^+(H_2O)_3$ with water vapor are shown in Figures 12 and 13, respectively.

One of the prominent feature of the winter hemisphere, shown in Figures 12 and 14, is the dominance of NO^+ above 79 km altitude. An increase in the cluster density compared to the total positive ion density N^+_{tot} is observed in the lower *D* region up to an altitude of 78 km. Above 78 km, the $H^+(H_2O)_n$ concentration decreases rapidly as a result of the decrease in the water vapor concentration and the increase in temperature (e.g., section 4). A similar dependence is also present in the NO^+ cluster family profile. Its concentration is related to the neutral nitric oxide density NO and to NO^+, respectively, at altitudes above 70 km. The abundance of the cluster family $NO^+ \cdot X$ is, however, only a minor part of the total positive ion density but, as expected, NO^+ represents the dominant positive ion above 80 km.

The corresponding situation in the summer hemisphere is shown in Figures 13 and 15. The differences from the winter profiles are evident, particularly above 80 km, where the H_2O concentration does not decrease as strongly with height as in the winter hemisphere. In addition, the lower summer *D* region temperatures enhance the rate of cluster formation. As a result, the proton-hydrated ions dominate the positive ion den-

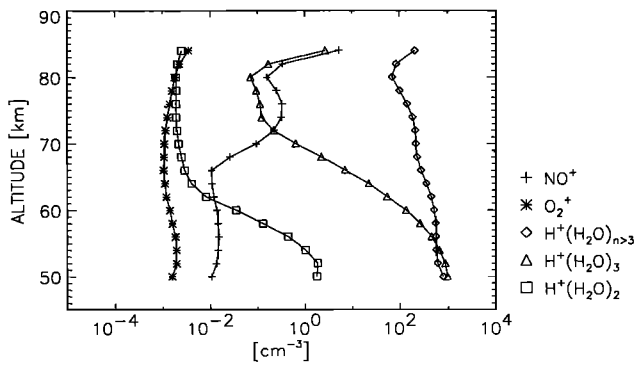

Figure 13. Vertical distribution of selected positive ions at the latitude −50° (summer hemisphere) for the height range of 50–84 km in January and noon conditions.

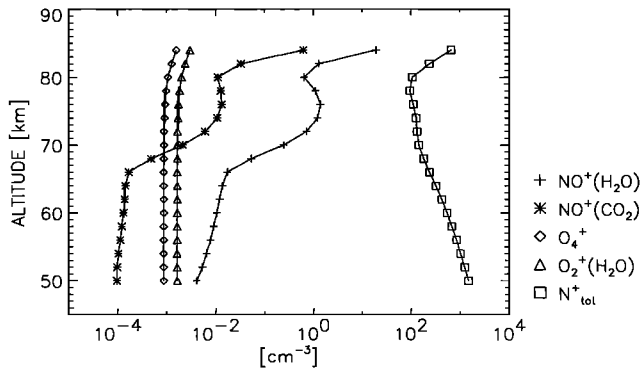

Figure 15. Vertical distribution of selected positive ions at the latitude −50° (summer hemisphere) for the height range of 50–84 km in January and noon conditions.

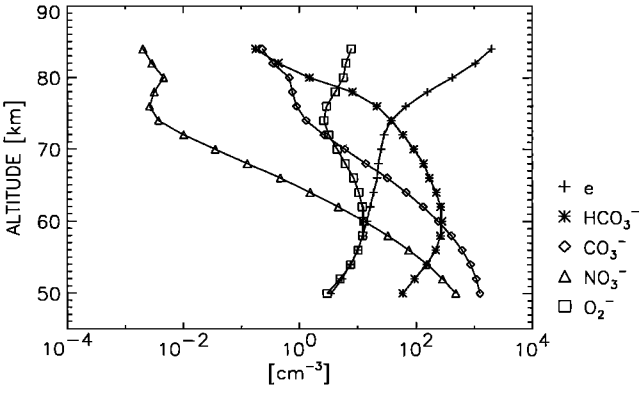

Figure 16. Vertical distribution of selected negative ions at the latitude 50° (winter hemisphere) for the height range of 50–84 km in January and noon conditions.

sity N_{tot}^+ over the whole range of the model from 50 to 84 km. The pronounced NO^+ cluster minimum on 66 and 80 km are the result of the minimum in the total ion production rate at these altitudes. In addition to these features, note that the distribution of positive ions is determined by a wide and complex variety of dependencies on mesospheric conditions.

6.6. Concentration of Selected Negative Ions

The main negative ions in our *D* region model are HCO_3^-, CO_3^-, NO_3^-, and O_2^-. Figures 16 and 17 show the height profiles of the main four negative ions together with the profiles of electrons and the total negative charge density for the January midday winter hemisphere (+50°) and summer hemisphere (−50°). The boundary above which the electron density dominates the total negative charge density N_{tot}^- ($\lambda = 1$) is found at an altitude between 74 and 75 km, showing almost no seasonal and latitudinal dependencies (see Figure 10). Although the ion HCO_3^- on mass 61 amu/*e* was regularly measured [e.g., *Arnold et al.*, 1971, 1982] many models describing the negative ion composition of the *D* region [e.g., *Thomas et al.*, 1973; *Burns et al.*, 1991] have not considered this ion in their model. Cl^- and some cluster ions of the chlorine ion may already play an important role. As in the case of the positive ions, the relative height dependence of individual ion species is strongly related to temperature and minor species concentrations in the mesosphere.

7. Parameterization of the Parameter f^+

The parameter f^+, which is of primary interest for modeling the general description of the positive ion distribution in the *D* region, is defined as the ratio of the sum of total cluster ions to the sum of the molecular ions NO^+ and O_2^+. It should be noted, that in the literature the f^+ value is sometimes defined as the ratio between the density of proton hydrates only to the two molecular ions. In the region of low water vapor mixing ratio (<1 ppmv) the two f^+ values can differ significantly.

Our model has also shown the importance of the water vapor mixing ratio on the f^+ value, particularly in the upper *D* region (>75–80 km). Therefore we are extending the proposed parameterization by *Kopp and Herrmann* [1984] with a dependence on the water vapor concentration, taking into account a third loss of cluster ions by collisional induced breakup. The extended parameterization of the ratio of cluster ions to molecular ions with the inclusion of H_2O besides the density ρ, temperature T, atomic oxygen O and electron concentrations, and the amount β of loss of cluster ions by collisional breakup is given by

$$f_{fit}^+ = A \frac{[\rho]^{n-1} k_1(T)[H_2O]}{g([O]) + \alpha[e] + \beta[\rho]^m k_2(T)}, \qquad (10)$$

where the function k_1 accounts for the dependencies on the temperature of the clustering chain in the forward direction, and the function k_2 in the backward direction. The function $g([O])$ takes into account the effect of the dissociative reaction

$$O_4^+ + O \rightarrow O_2^+ + O_3 \qquad (11)$$

on the cluster formation involving O_2^+. The parameters m and n related to the neutral density $[\rho]$ include the dependencies of the clustering chain on the attachment or collisional induced breakup type; i.e., they should assume numerical values between 1 and 3.

For the condition used in our model with relatively low atomic oxygen density ($[O] < 10^{10}$ cm^{-3}) it is possible to simplify the extended parameterization of f^+ by neglecting by setting $g([O]) = 0$. This also means, that the main cluster formation is the O_2^+- and not the NO^+-hydration and we can use $n = 2$, a number which takes into account the two body reactions in the O_2^+-clustering chain. The temperature dependence in the oxygen ion hydration of the forward reaction k_1 is proportional to T^{-3}.

In order to determine the parameters in (10), we performed a fit of the analytical expression (10) to the actual values of f^+ as obtained from a separate model calculation based on the January midday winter hemisphere but involving an artificial modified H_2O density profile ranging over many orders of magnitude. With a mean dissociative recombination coefficient $\alpha = 4 \times 10^{-6}$ cm^3 s^{-1}, the fit yields

$$f_{fit}^+ = 4.36 \times 10^{-12} \frac{[\rho]^{0.6} T^{-3}[H_2O]}{4 \times 10^{-6}[e]} \qquad (12)$$

where the concentrations are in units cm^{-3}. The exponent $n - 1$ is below 1, a result which takes into account the possibility of neglecting the collision-induced breakup β in the denominator of (10). The comparison between f_{fit}^+ profile and the profile f^+ determined by the model calculation is shown in Figure 18. Note the excellent agreement over many orders of magnitude.

Equation (10) together with the parameters determined

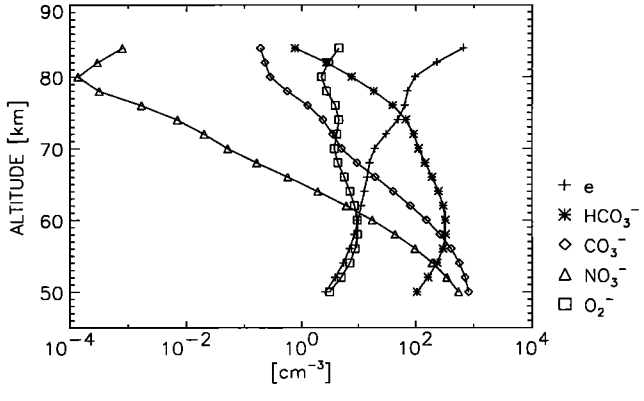

Figure 17. Vertical distribution of selected negative ions at the latitude −50° (summer hemisphere) for the height range of 50–84 km in January and noon conditions.

from the model calculation using an arbitrary modified H_2O density profile is used to estimate the f^+ profile for different mesospheric conditions. Figure 19 shows two comparisons between f^+_{fit} and f^+. The first pair of profiles is based on January midday summer hemisphere conditions at +50°, while the second pair reflects September midday conditions at the equator. In both situations, reasonably good agreement is obtained. This implies that the location of the transition height ($f^+ = 1$) at midlatitudes is determined mainly by the concentration of the water vapor and the electron concentration. Consequently, the water vapor at the transition height may be inferred from a measurement of the electron concentration. The approximation based on (10) and (12), respectively, yields

$$[H_2O] = 1.09 \times 10^{-6}[\rho]^{0.6}T^{-3}[e] \quad (13)$$

where the units of the water vapor $[H_2O]$, the air density $[\rho]$, and the electron concentration $[e]$ are in cm^{-3} and the temperature T is in degrees kelvin.

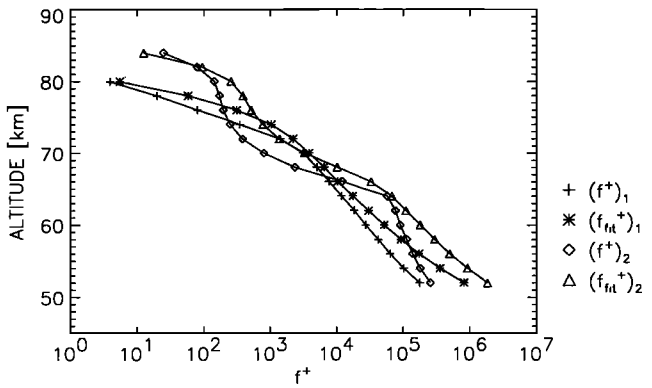

Figure 19. Approximation of f^+ profiles derived from (11) with the parameter values fixed by the fit shown in Figure 18 (see text). The first pair of profiles (index 1) is based on January midday summer hemisphere conditions at +50° while the second pair (index 2) reflects September midday conditions at 0°. For both the situations a reasonable good estimation is obtained.

8. Comparison With in Situ Measurements and IRI-90

A comparison of our model results with in situ rocket measurements of electron, total positive and negative ion density as well as with electron profiles infered from ground based ionosondes is difficult. Below 84 km, the ionosonde data are restricted to daytime situations and events with enhanced ionization by corpuscular radiation. Ionosonde electron profiles in the D region have also a characteristic theoretical bottom shape which may deviate significantly from real profiles. Despite a large number of relieable electron profiles obtained from rocket measurements, which are available for comparison, it is still difficult to associate them reasonably well to a daily-averaged electron density profile. In addition, at heights between 50 and 70 km electrons are minor constituents among the negatively charged species. Thus, for a comparison of our model data with electron data from rockets, we expect some deviations, particularly below 70 km altitude.

A selection of daytime electron density profiles from five rocket flights at midlatitudes (37°–40°N) is shown in Figure 20, together with an average midlatitude winter-time electron density profile at noon. In this comparison, the model electron density is about one order of magnitude lower than obtained from rocket measurements. Conditions at midlatitudes in January are particularly suitable for the occurrence of a frequent situation known as winter anomaly. This situation is characterized by an enhancements of both temperature and the nitric oxide density in the mesosphere and a related increase of the D region electron density best seen in the increase of radio wave absorption in the 2–3.5 MHz band. The much lower electron density of our model in January at midlatitude may thus indeed reflect an underestimation of the mesospheric nitric oxide density. A further comparison of four rocket electron density profiles with our model at equinox is given in Figure 21. The agreement here between model and measurements is much better, although the model results may still reflect a lower limit of the actual nitric oxide densities, and an underestimation of the ion production due to the neglection of the O_2^+ ion contribution from $O_2(^1\Delta)$ is probable.

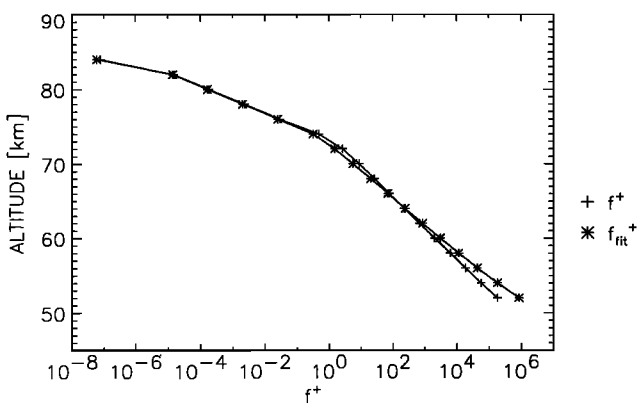

Figure 18. Fit of the expression (11) to the actual values of f^+ as obtained from a separate model calculation based on the January midday winter hemisphere at 50° but involving an artificial modified H_2O density profile. For the parameter values obtained, see text.

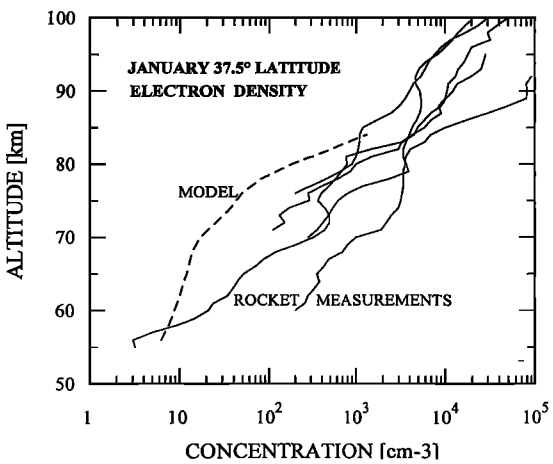

Figure 20. Five daytime electron density rocket profiles (solid curves) from M. Friedrich and K. M. Torkar (private communication, 1996) in January at 37°–40°N (rocket flights F43, F14.440, F14.381, F15.5, and S56A-1), and the corresponding model electron density profile of January 15 at noon (dashed curve).

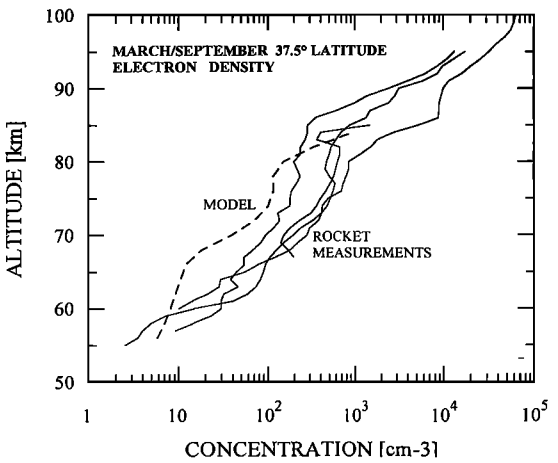

Figure 21. Four daytime electron density rocket profiles (solid curves) in March (equinox) at 37–40°N (rocket flights F14.435, F14.107, F14.244, and F14.395) from Friedrich and Torkar (1996), and the corresponding model electron density profile of March 15 at noon (dashed curve).

In order to compare the relative abundance of electrons with respect to the total negative charge density we use some of the few simultaneous rocket measurements of positive and negative ion composition by the Max Planck Institute of Heidelberg [*Arnold and Krankowsky*, 1977] at Arenosillo (37°N), Kiruna (67.9°N), and Andoya (69.3°N). The height profiles of the parameter λ deduced from the measured N^+_{tot}/N^-_{tot} ratio in four rocket flights in winter by *Arnold and Krankowsky* [1977] and a selected profile with λ values from our model for midday in January at 50°N are shown in Figure 22. The large λ values at altitudes between 70 and 80 km are explained by large error bars in case the ratio N^+_{tot}/N^-_{tot} is close to one. From this comparison, a systematic deviation between measured and modeled λ values is not obvious. Despite of the large variability of measured λ values it is still possible to claim a fair agreement between model and measurements for the ratio of negative ions to electrons.

A further comparison between three measured height profiles of the parameter f^+ from positive ion composition measurements in winter at 37°N (Arenosillo, Spain) by *Arnold and Krankowsky* [1979] and 50.3°N (Red Lake, Canada) by *Kopp and Herrmann* [1984], and the two corresponding model profiles for midday are shown in Figure 23. A considerable discrepancy between model and measurements is evident. The higher f^+ values of the model are to some extend an effect of the longer lifetime caused by lower electron concentrations in our wintertime model as seen in Figure 20. In addition, all three measurements (winter anomaly and auroral events) had higher temperatures in the mesosphere as used by the model, which leads to an increase of cluster breakup and lower f^+ values in the measurements. However, it is also possible that part of the high f^+ values in our model is due to larger mesospheric water vapor concentration in winter and/or to an underestimation of the temperature dependence of the cluster breakup reaction constants in our ion chemical model. The effect from different temperatures between model and measurements or the errors in the temperature dependence of the cluster breakup reaction rate constant are probably the two main reasons to explain the larger f^+ values in our model.

From the most recent International Reference Ionosphere (IRI-90) electron densities are available to heights as low as 66 km [*Bilitza*, 1990]. However, these data are based on a limited number of in situ measurements from which an analytical expression for the characteristic point of the *D* layer has been deduced at a fixed altitude of 81 km. Figure 24 presents the comparison of the electron density as calculated for January noon conditions and the corresponding electron density according to IRI-90 data. Considering Figure 24 we first note, that the IRI-90 electron density data is lacking features associated with the galactic cosmic rays as observed in the model calculation. Neither the variability with the latitude nor an ionization background due to galactic cosmic rays can be in the IRI. Second, in the winter hemisphere a clear augmentation of the electron density above 75 km due to high NO densities is missing. And, third, the characteristic augmentation of the electron density in the transition region between *D* and *E*

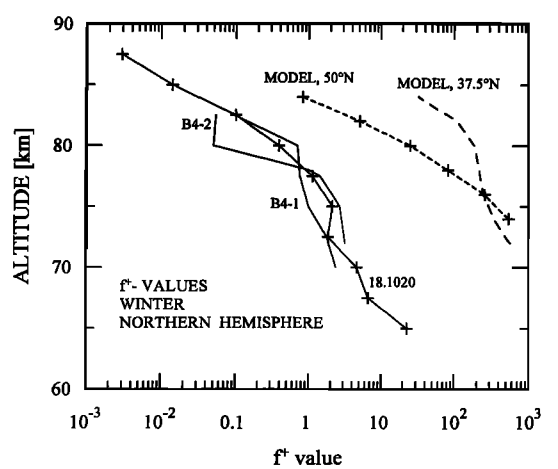

Figure 22. Four profiles of the ratio $\lambda = [N^-_{tot}]/[e]$ deduced from the measurements of positive and negative ion composition in winter at Arenosillo (37°N), Esrange (67.9°N), and Andoya (69.3°N) by *Arnold and Krankowsky* [1977], and the corresponding midday model profile of January 15 at 50°N.

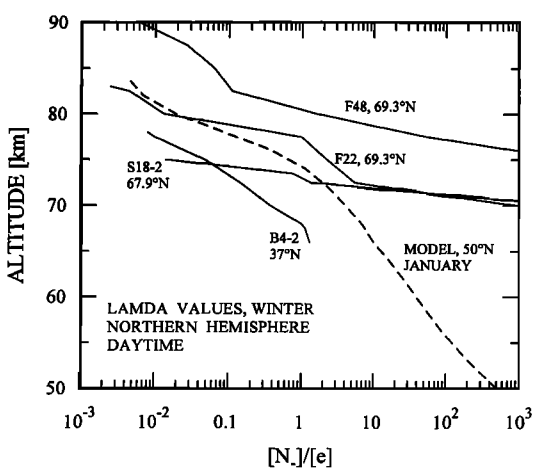

Figure 23. Three daytime profiles of the parameter $f^+ = [Clust^+]/\{[NO^+] + [O_2^+]\}$ in winter from positive ion composition measurements at Arenosillo (rocket flights B4-2 and B4-1) and Red Lake (rocket flight 18.1020), and the corresponding model profiles at noon for latitudes 37.5°N and 50°N, respectively.

region is also not observed. Because of the missing of these expected features, the broad discrepancy between model calculation and IRI-90 data as indicated by Figure 24 should not be stressed too much. This point of view is supported by the comparison of in situ electron density measurements with the modeled electron density which yields a broader agreement.

The electron density calculated by the present model calculation is up to a factor 10 lower than the corresponding IRI-90 electron density data. This discrepancy is too big as to be explained by the missing ionization of $O_2(^1\Delta)$ by Lyman β. Clearly, more work on both subjects, the IRI-90 data and the present model calculation, is necessary in order to resolve the discussed discrepancies.

9. Conclusions

An ion chemical steady state model of the positive and negative ion profiles of the *D* region has been presented. It is based on a compilation of ion-chemical reaction rate constants [*Kopp*, 1996] and mesospheric data from a two-dimensional neutral model [*Granier and Brasseur*, 1992]. The model ranges from the stratopause (50 km) to the mesopause (84 km) and from 50°S to 50°N latitude. It incorporates a total of about 400 ion and photochemical reactions. The ion production includes direct photoionization of NO by Lyman α above 60 km and by galactic cosmic rays between 50 and 80 km. The ionization of $O_2(^1\Delta)$ by Lyman β is not included. The main neutral constituents in the model are N_2, O_2, CO_2, CH_4, H_2, H_2O, and, as photochemically active species, $O(^3P)$, NO, O_3, and H. Primary positive ions are NO^+, O_2^+, O^+, N^+, and N_2^+, negative ions are O^- and O_2^-. As secondary positive ions the model includes all possible intermediate clusters of the form $O_2^+ \cdot X$, $NO^+ \cdot X$ and proton hydrates $H^+(H_2O)_{2-7}$. Besides electrons, the negative secondary ions O_3^-, CO_3^-, NO_2^-, OH^-, NO_3^-, CO_4^-, O_4^-, and HCO_3^- are considered.

The model calculation yields detailed information about the density distribution of the considered ion species as a function latitude and altitude. A pronounced difference between summer and winter hemispheres is found. For most cases, this is the result of changes in the mesospheric trace gas concentrations and in the ionization conditions.

The f^+ parameter, the most important model parameter for the positive ion chemistry of the *D* region, reaches unity at a level which defines the transition height between the *D* region and the *E* region. In our model, this transition is located below 84 km altitude, which is the upper limit of our model, only in the winter hemisphere north of 40°N. In general, the transition height at midlatitudes is located above 84 km. The model shows an important dependency of the f^+ value on the water vapor mixing ratio. As a consequence, the proposed parameterization by *Kopp and Herrmann* [1984] is extended to include a dependence on the water vapor concentration, and taking into account a third process for loss of cluster ions by collisional induced breakup. The new proposed parameterization agrees reasonably well with the f^+ values calculated from the model and offers the possibility to infer the water vapor concentration at the transition height from the knowledge of the electron density.

The discrepancies between modeled electron density, the f^+ and the λ parameters and measurements taken from a selection of rocket flights and the IRI-90 model reflect a possible underestimation of the used nitric oxide density in the mesosphere, particularly for midlatitudes in winter. A comparison

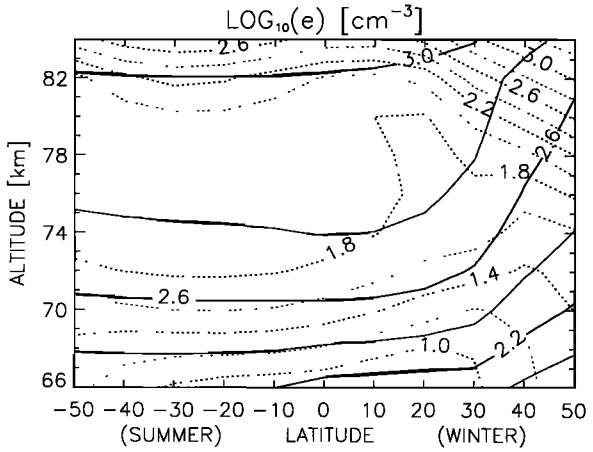

Figure 24. Comparison of the modeled (dotted line) and the IRI-90 electron density (solid line) in the *D*-region for the height range of 50–84 km and between the latitudes −50° (summer hemisphere) and 50° (winter hemisphere) for January and noon condition. For the discussion, see text.

of the nitric oxide densities in January with the 1992 sunset data of HALOE shows in general much lower NO number densities in our model above 65–70 km altitude, particularly at latitudes between 35°N and 50°N. The model also indicates the need to introduce in the future IRI space *D* region model a seasonal and height-dependent electron density profile related to the variability of NO and H_2O concentrations.

Acknowledgments. This work is supported by the Swiss National Science Foundation. The National Center for Atmospheric Research is sponsored by the U.S. National Science Foundation. Part of the work of A.K. has been performed at Max-Planck-Institute for Extraterrestrial Physics. We thank M. Friedrich and K. M. Tokar for providing us data of electron density measurements and are grateful to an unknown referee for constructive criticism.

The Editor thanks J. A. Fennelly and another referee for their assistance in evaluating this paper.

References

Andrews, D. G., and M. E. McIntyre, Planetary waves in horizontal and vertical shear: The generalized Eliassen-Palm relation and the mean zonal acceleration, *J. Atmos. Sci.*, *33*, 2031–2048, 1976.

Arnold, F., and D. Krankowsky, Ion composition and electron- and ion-loss processes in the Earth's atmosphere, in *Dynamical and Chemical Coupling*, edited by B. Grandal and J. H. Holtet, pp. 93–127, D. Reidel, Norwell, Mass., 1977.

Arnold, F., and D. Krankowsky, Mid-latitude lower ionosphere structure and composition measurements during winter, *J. Atmos. Terr. Phys.*, *41*, 1127–1140, 1979.

Arnold, F., J. Kissel, D. Krankowsky, H. Wieder, and J. Zähringer, Negative ions in the lower ionosphere: A mass-spectrometric measurement, *J. Atmos. Terr. Phys.*, *33*, 1169–1175, 1971.

Arnold, F., A. A. Viggiano, and E. E. Ferguson, Combined mass spectrometric composition measurements of the positive and negative ions in the lower ionosphere, II, Negative ions, *Planet. Space Sci.*, *30*, 1307–1314, 1982.

Bilitza, D., International Reference Ionosphere 1990, *Rep. NSSDC/WDC-A-R&S 90-20*, Natl. Sci. Data Cent., Greenbelt, Md., 1990.

Brasseur, G., and P. De Beats, Ions in the mesosphere and lower thermosphere: A two-dimensional model, *J. Geophys. Res.*, *91*, 4025–4046, 1986.

Brasseur, G., and P. C. Simon, Stratospheric chemical and thermal response to long-term variability in solar UV irradiance, *J. Geophys. Res.*, *86*, 7343–7362, 1981.

Brasseur, G., and S. Solomon, Aeronomy of the middle atmosphere, 2nd ed., D. Reidel, Norwell, Mass., 1986.

Brasseur, G., M. H. Hitchman, S. Walters, M. Dymek, E. Falise, and M. Pirre, An interactive chemical dynamical radiative two-dimensional model of the middle atmosphere, *J. Geophys. Res.*, *95*, 5639–5655, 1990.

Briegleb, B. P., Longwave band model for thermal radiation in climate studies, *J. Geophys. Res.*, *97*, 11475–11485, 1992.

Burns, C. J., E. Turunen, M. Matveinen, H. Ranta, and J. K. Hargreaves, Chemical modeling of the quiet summer *D*- and *E*-region using EISCAT electron density profiles, *J. Atmos. Terr. Phys.*, *53*, 115–134, 1991.

Conley, T. D., E. R. Hegblom, and R. S. Narcisi, *D*-region positive and negative ion concentration and mobilities during the February 1979 eclipse, *J. Atmos. Terr. Phys.*, *45*, 499–513, 1983.

DeMore, W. P., S. P. Sander, D. M. Golden, R. F. Hampson, M. J. Kurylo, C. J. Howard, A. R. Ravishankara, C. E. Kolb, and M. J. Molina, Chemical kinetics and photochemical data for use in stratospheric modeling, evaluation number 10, *JPL Publ.*, *92-20*, 1992.

Fehsenfeld, F. C., and E. E. Ferguson, On the origin of water cluster ions in the *D*-region, *J. Geophys. Res.*, *24*, 2217–2222, 1969.

Ferguson, E. E., and F. C. Fehsenfeld, Water vapor ion cluster concentrations in the *D*-region, *J. Geophys. Res.*, *24*, 5743–5751, 1969.

Gear, C. W., Numerical initial value problems in ordinary differential equations, in *Automatic Comput. Ser.*, pp. 67–73, Prentice Hall, Englewood Cliffs, N. J., 1971.

Granier, C., and G. Brasseur, Impact of heterogeneous chemistry on model predictions of ozone changes, *J. Geophys. Res.*, *97*, 18015–18033, 1992.

Heaps, M. G., A parameterization of cosmic ray ionization, *Planet. Space Sci.*, *26*, 513–517, 1978.

Hunten, D. M., and M. B. McElroy, Metastable $O_2[^1\Delta]$ as a major source of ions in the *D*-region, *J. Geophys. Res.*, *73*, 2421–2428, 1968.

Kopp, E., Mesospheric H_2O and H_2O_2 densities inferred from in situ positive ion composition measurement, *Adv. Space Res.*, *4*(6), 13–18, 1984.

Kopp, E., Electron and ion densities, in *The Upper Atmosphere, Data Analysis and Interpretation*, edited by W. Dieminger, G. K. Hartman, and R. Leitinger, pp. 625–635, Springer, New York, 1996.

Kopp, E., and U. Herrmann, Ion composition in the lower ionosphere, *Ann. Geophys.*, *2*(1), 83–94, 1984.

Koshelev, V. V., The winter anomaly in the ionospheric *D*-region—Some numerical calculations, *J. Atmos. Terr. Phys.*, *49*, 81–97, 1987.

Millar, T. J., J. M. C. Rawlings, A. Bennett, P. D. Brown, and S. B. Charnley, Gas phase reactions and rate coefficients for use in astrochemistry, The UMIST rate file, *Astron. Astrophys. Suppl. Ser.*, *87*, 585–619, 1991.

Narcisi, R. S., and A. D. Bailey, Mass spectrometric measurements of positive ions at altitudes from 64 to 112 km, *J. Geophys. Res.*, *70*, 3687–3700, 1965.

Narcisi, R. S., A. D. Bailey, L. Della Lucca, C. Sherman, and D. M. Thomas, Positive and negative ion composition measurements in the *D*- and *E*-region during the solar eclipse of 26 February 1979, *J. Atmos. Terr. Phys.*, *45*, 461–478, 1983.

Rakshit, A. B., and P. Warnek, A drift chamber study of the formation of water cluster ions in oxygen, *J. Chem. Phys.*, *73*, 5074–5080, 1980.

Reid, G. C., Ion chemistry in the *D*-region, *Adv. Atomic Molecular Phys.*, vol. 12, edited by D. R. Baets and D. R. Bederson, pp. 375–413, Academic, San Diego, Calif., 1976.

Reid, G. C., The production of water cluster ions in the quiet daytime, *Planet. Space Sci.*, *25*, 275–290, 1977.

Rusch, D. W., J. C. Gerard, S. Solomon, P. J. Crutzen, and G. C. Reid, The effect of particle precipitation events on the neutral and ion chemistry of the middle atmosphere, 1, Odd nitrogen, *Planet. Space Sci.*, *29*, 767–774, 1981.

Swider, W., and R. S. Narcisi, Steady state model of the *D*-region during February 1979 eclipse, *J. Atmos. Terr. Phys.*, *45*, 493–498, 1983.

Thomas, L., NO^+ and water cluster ions in the *D*-region, *J. Atmos. Terr. Phys.*, *38*, 61–67, 1976a.

Thomas, L., Mesospheric temperatures and the formation of water cluster ions in the *D*-region, *J. Atmos. Terr. Phys.*, *38*, 1235–1350, 1976b.

Thomas, L., Modeling the ion composition of the middle atmosphere, *Ann. Geophys.*, *1*, 61–73, 1983.

Thomas, L., and M. R. Bowman, Model studies of the *D*-region negative-ion composition during day-time and night-time, *J. Atmos. Terr. Phys.*, *47*, 547–556, 1985.

Thomas, L., P. M. Gondhalekar, and M. R. Bowman, The negative-ion composition of the daytime *D*-region, *J. Atmos. Terr. Phys.*, *35*, 397–404, 1973.

Wisemberg, J., and G. Kockarts, Negative ion chemistry in the terrestrial *D*-region and signal flow graph theory, *J. Geophys. Res.*, *84*, 4642–4652, 1980.

G. Brasseur and C. Granier, National Center of Atmospheric Research, Boulder, CO 80307.

E. Kopp and A. Kull, Physikalisches Institut der Universität Bern, Sidlerstrasse 5, CH-3012 Bern, Switzerland. (e-mail: kopp@phim.unibe.ch)

(Received June 18, 1996; revised January 30, 1997;
accepted January 31, 1997.)